

A short study on ptychography

Unathi Skosana

July 6, 2021

Contents

<i>1</i>	<i>Coherent diffraction imaging</i>	<i>2</i>
<i>1.1</i>	<i>Ptychography</i>	<i>2</i>
<i>1.2</i>	<i>Ptychography iterative engine</i>	<i>3</i>
<i>1.3</i>	<i>The extended ptychographic engine (ePIE)</i>	<i>4</i>
<i>1.4</i>	<i>Image resolution within ptychography</i>	<i>5</i>
<i>2</i>	<i>Ptychography with different update functions</i>	<i>7</i>
<i>2.1</i>	<i>Ptychography iterative engine (PIE)</i>	<i>7</i>
<i>2.2</i>	<i>Extended ptychography iterative engine (ePIE)</i>	<i>9</i>
<i>3</i>	<i>Quantitative rule of thumb for algorithmic convergence</i>	<i>9</i>
<i>4</i>	<i>Enhancements of the ptychography iterative engine</i>	<i>11</i>
<i>5</i>	<i>With different probing beams</i>	<i>12</i>
<i>5.1</i>	<i>Laguerre-Gaussian modes</i>	<i>13</i>
<i>6</i>	<i>With experimental errors</i>	<i>14</i>
<i>6.1</i>	<i>Shot noise</i>	<i>15</i>
<i>6.2</i>	<i>Random noise</i>	<i>15</i>

1 Coherent diffraction imaging

SINCE THEIR ADVENT, *coherent diffractive imaging* (CDI) methods - an image of a specimen is constructed directly from how the specimen diffracts a highly coherent illumination/light source without the need for image-forming optics — have gained considerable appeal, in antithesis to conventional microscopy methods which employ optics (a system of lenses) between the specimen and detector to form an image of the specimen ¹. However, imaging specimens in this way presents challenges of its own, in the recording of the diffraction patterns (intensity measurement) by a detector (CCD camera), virtually all phase information ² of light transmitted through the specimen is lost. Thus CDI methods are tasked with computationally reconstructing the phase of a specimen that satisfies a set of constraints posed by the measured diffraction patterns, such computational methods are collectively called *phase retrieval* algorithms.

Ptychography [2] is one member of the family of iterative phase retrieval algorithms that has gained considerable popularity. The modus operandi of ptychographic techniques is of a simple nature, a light source (probe) illuminates some known region on the specimen (sample), the resulting diffraction pattern is collected in the *Fraunhofer regime*, and the illumination region is then shifted literally on the specimen to a neighboring known region on the specimen, and the process is repeated in an iterative manner, spanning however large of a field of view region on the specimen, the only requirement being that neighboring illumination regions must have an overlap and the probe be localised and remain constant as it moves relative to the sample. In antithesis to conventional iterative phase retrieval algorithms (which use one diffraction pattern taken from a spatially isolated object), no a priori knowledge about the sample size is necessary, and the illuminating probe is not restricted to any form [3]. The robustness and efficacy of ptychographic techniques is a consequence of the overlap requirement between neighboring illumination regions, this condition introduces some redundancy in the data set, which then relaxes some constraints in the original problem, leading to an overdetermined phase retrieval problem [4].

1.1 Ptychography

We now describe the generic procedure of ptychographic algorithms. An illumination probe described by a 2-dimensional complex (amplitude and phase) function $P(x)$, scans an object described by another 2-dimensional complex function $O(x)$ ³. As mentioned before, the

¹ For this reason, CDI methods are often cited as being more dose-efficient since only a few, potentially signal degrading optics, are between the light source, specimen and detector.

² The relative phase change of the transmitted light contains information about path followed by light through the specimen, encoding properties of the specimen such as the thickness, depth and refractive index of the specimen [1].

³ This approximation is well suited for thin objects.

probe P and object O can be moved relative to each; let \mathbf{y} be such a relative shift between the probe and object. The propagated wave, called the exit wave $\psi(x)$, immediately after the sample is a *Hadamard product* between the probe function at $P(\mathbf{x} - \mathbf{y})$ and sample function at $O(\mathbf{x})$

$$\psi(\mathbf{x}) = P(\mathbf{x} - \mathbf{y}) \odot O(\mathbf{x}). \quad (1)$$

If diffraction patterns are observed at the Fraunhofer regime ⁴, then the intensity measured by the detector is given by

$$I(\mathbf{q}) = |\mathcal{F}[P(\mathbf{x} - \mathbf{y}) \odot O(\mathbf{x})]|^2, \quad (2)$$

where \mathbf{q} is a suitable spatial frequency (reciprocal-space) in the real-space image and \mathcal{F} is the 2D *Fourier transform*. Worthy to note is that the above diffraction pattern does not uniquely correspond with $P(\mathbf{x} - \mathbf{y}), O(\mathbf{x})$, for instance

$$\begin{aligned} P'(\mathbf{x} - \mathbf{y}) &= cP(\mathbf{x} - \mathbf{y}) \\ O'(\mathbf{x}) &= c^{-1}O(\mathbf{x}), \end{aligned} \quad (3)$$

where c is constant will also satisfy Eq. 2. Also if the P and O are shifted a constant offset \mathbf{a} ,

$$\begin{aligned} P'(\mathbf{x} - \mathbf{y}) &= P(\mathbf{x} - \mathbf{y} - \mathbf{a}) \\ O'(\mathbf{x}) &= O(\mathbf{x} - \mathbf{a}), \end{aligned} \quad (4)$$

the Fourier transform is invariant under such offsets such that the above will also satisfy Eq. 2. The goal of a ptychographic reconstruction is thus to associate such a recorded diffraction pattern of the form Eq. 2] with a correct phase, and then via an inverse Fourier transform recover O (and possibly P), though not uniquely as already highlighted by the aforementioned ambiguities. We next describe such an algorithm briefly.

1.2 Ptychography iterative engine

The ptychography iterative engine (PIE) algorithm as described in Ref. [2] proceeds as follows:

- i Begin with a guess of object function (free space) at $\mathbf{x}, O_j(\mathbf{x})$, the subscript j_{th} iteration of the algorithm.

⁴ Often called the far field, the field with a wavelength λ propagating through an aperture of diameter D is observed at a distance z such that $z \gg \frac{\pi D^2}{4\lambda}$

- ii Propagate the illumination function at the current position $\mathbf{y}_j, P(\mathbf{x} - \mathbf{y}_j)$ through guessed object function $O_j(\mathbf{x})$; Producing a guess for the exit wave function

$$\psi_j(\mathbf{x}) = O_j(\mathbf{x}) \odot P_j(\mathbf{x} - \mathbf{y}_j) \quad (5)$$

- iii Fourier transform the guessed exit wave to the diffraction plane and replace it's square modulus with that of the j_{th} recorded diffraction pattern $I_j(\mathbf{q})$ so

$$\Psi_j(\mathbf{q}) = \sqrt{I_j(\mathbf{q})} \frac{\mathcal{F}[\psi_j(\mathbf{x})]}{|\mathcal{F}[\psi_j(\mathbf{x})]|} \quad (6)$$

- iv Perform the inverse Fourier transform to recover the updated exit-wave

$$\psi'_j(\mathbf{x}) = \mathcal{F}^{-1}[\Psi_j(\mathbf{q})] \quad (7)$$

- v Update the guessed object function

$$O_{j+1}(\mathbf{x}) = O_j(\mathbf{x}) + \frac{|P_j(\mathbf{x} - \mathbf{y}_j)| |P_j^*(\mathbf{x} - \mathbf{y}_j)|}{|P_j(\mathbf{x} - \mathbf{y}_j)|_{\max} (|P_j(\mathbf{x} - \mathbf{y}_j)|^2 + \alpha |P_j(\mathbf{x} - \mathbf{y}_j)|_{\max}^2)} (\psi'_j(\mathbf{x}) - \psi_j(\mathbf{x})) \quad (8)$$

where α is a tuning parameter of the update function.

- vi Move to the next position \mathbf{y}_{j+1} which satisfies the overlap requirement, and repeat steps (ii)-(v) until we have ran through all the positions and measured diffraction patterns. This entire process is then repeated again to the desired number of iterations.

The \mathbf{y}_j and their corresponding diffraction patterns $I_j(\mathbf{q})$ can also be accessed in a random sequence $\sigma(j)$ instead, either to prevent the emergence of periodic artefacts in the reconstruction or introduce random fluctuations that reduce stagnation.

1.3 The extended ptychographic engine (ePIE)

Since PIE as described by Rodenburg and Faulkner, ptychographic algorithms have shown rapid progress, that it is now possible to reconstruct both the object function O and illumination function P . The extended ptychographic engine (ePIE) [5] is improvement

upon PIE algorithm, which additionally retrieves both object and illumination functions. The operation of ePIE is similar to that of PIE as described in the previous section, the algorithm begins with initial guesses of both object function and probe function, the initial object function can be taken to be empty while it helps to have some rough approximation of the shape of the probe *i.e.* support function of the intensity region of probe but not entirely necessary. The update function of step (v) is modified and an additional step is sandwiched between step (v) and (vi) as such:

v Update the guessed object function

$$O_{j+1}(\mathbf{x}) = O_j(\mathbf{x}) + \alpha \frac{P_j^*(\mathbf{x} - \mathbf{y}_j)}{|P_j(\mathbf{x} - \mathbf{y}_j)|_{\max}^2} (\psi'_j(\mathbf{x}) - \psi_j(\mathbf{x})) \quad (9)$$

vi Update the guessed probe function

$$P_{j+1}(\mathbf{x}) = P_j(\mathbf{x}) + \beta \frac{O_j^*(\mathbf{x} + \mathbf{y}_j)}{|O_j(\mathbf{x} + \mathbf{y}_j)|_{\max}^2} (\psi'_j(\mathbf{x}) - \psi_j(\mathbf{x})) \quad (10)$$

where β is tuning parameter for the probe update function, similar in role to α for the object update function.

The update functions of ePIE can possibly be ill-conditioned; if both the initial guesses of O_j and P_j are empty space (0-valued pixels) then the updated probe and object functions diverge. One possible way to circumvent such as scenario is to assign the initial probe guess to be populated with 1-valued pixels (normalized) then for a first few iterations only the object function is updated while the probe is held fixed such that when the probe eventually gets updated the object function is no longer empty space.

1.4 Image resolution within ptychography

In the view of the fact that CDI methods are based on the phenomenon of diffraction, thus any factor that could possibly have an influence on the collected the diffraction patterns will likely have an somewhat of an influence on the resolution of the reconstructed images. These can include physical factors that influence the phenomenon of diffraction and detector's specifications, we will briefly look at some of these factors.

DETECTOR'S DYNAMIC RANGE is defined as the difference between its noise and saturation intensity, which represents the spectrum of intensities that are discernible by the detector, intensities above the

saturation threshold are indistinguishable and intensities comparable to the noise will be indistinguishable to noise. For instance, for a CCD camera is determined by *full well capacity* (maximum electron count before a pixel on the detector is saturated) and system noise (dark and read noise), defined as:

$$\text{DR} = 20 \log_{10} \left(\frac{n_{\text{full-well}}}{n_{\text{noise}}} \right) \quad (11)$$

measured in decibels. For a CCD camera with a full well capacity of 40,000 electrons and a system noise of 8 electrons gives a dynamic range of

$$\text{DR} = 20 \log_{10} \left(\frac{40,000}{8} \right) \approx 74 \text{ dB} \quad (12)$$

A quick glance at the intensity of the Fraunhofer diffraction pattern (in cylindrical coordinates) collected at a distance z from a circular aperture of diameter D is given by

$$I(\rho, z) = I_0 \left(\frac{\pi D^2}{4\lambda z} \right)^2 \left[2 \frac{J_1(kD\rho/2z)}{(kD\rho/2z)} \right]^2, \quad (13)$$

where λ is the wavelength of the light source, $k = \frac{2\pi}{\lambda}$ the corresponding wave vector and the first order Bessel function [6]. We show proportionally factor in the squared brackets in Fig. 1.4, we observe that the first peak intensity (normalized) is much more pronounced than the other peaks, giving a high dynamic range (maximum difference between peak values). Some experimental realizations of the ptychographic algorithms have devised ways reduce this dynamic range, Ref. [5] suggested recording multiple diffraction patterns for each scanned position at increasing exposure times and then recombined and average the patterns, and Ref. [1] placed a diffuser over the circular aperture to lower dynamic range ten-fold.

WAVELENGTH OF THE SOURCE AND GEOMETRY OF THE OPTICS determines whether any two features on a specimen can be distinguished from one another by their diffraction patterns by imposing a stringent condition called the *Rayleigh criterion*. Lord Rayleigh's criterion requires that the diffraction patterns of two such features must be such that the distance between their peaks is more than the distance between the peak of one pattern to the first zero of the other peak [6] as shown Fig. 1.4. The location of the first zero of Eq. 13 is at 1.22π , which gives

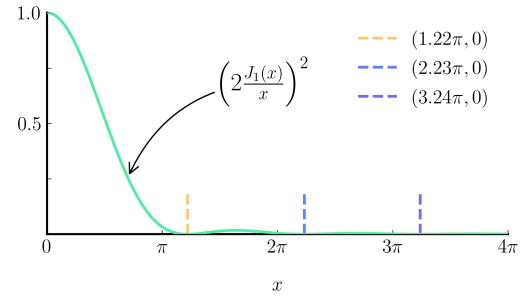


Fig. 1 Square of the Jinc function, where J_1 is first order Bessel function.

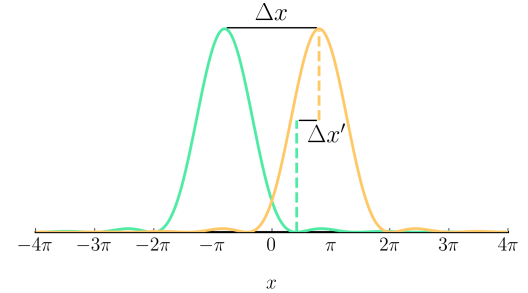


Fig. 2 Rayleigh criterion requires that the distance Δx be greater than $\Delta x'$ for the two diffraction patterns (peaks) to be distinguishable.

$$\frac{kD\rho}{2z} = 1.22\pi,$$

$$\frac{\rho}{z} = \frac{1.22}{D} \frac{2\pi}{k} = \frac{1.22\lambda}{D}. \quad (14)$$

Here the ratio $\frac{\rho}{z}$ is associated with a minimum angle θ_{min} , which depends on the wavelength λ and diameter of the circular aperture D . Thus the angle between the diffraction patterns (peaks) has to be at least θ_{min} if they are to be resolved.

NOISE in the collected diffraction patterns from various noise sources⁵ can negatively influence the images reconstructed from aforesaid diffraction patterns. We will look at some of the noise sources and the robustness of the ptychographic algorithms against some of these sources in detail in the section that follow.

⁵ Imperfect optics, imperfect alignment of optics, system noise, background noise etc

2 Ptychography with different update functions

IN ORDER TO INVESTIGATE the effectiveness of the methods described previously, one can lift the limitations that hinder the success of the algorithm, posed by physical realization by considering an idealized scenario where the far-field diffraction patterns are simulated. We shall return to the investigation of some of these errors at a later section. However, for now we consider an idealized situation where we have the simulated probing beam is highly coherent and does not suffer from any shot noise and we also assume perfect knowledge our probing beam and its probing positions. We first consider the ptychography iterative engine (PIE) algorithm

2.1 Ptychography iterative engine (PIE)

Two 8-bit 256 by 256 pixels images are used to represent the object of interest's amplitude and phase profiles. The two images are read in as 2D arrays with values in the range [0, 0, 1.0], the amplitude profile left unchanged and the phase profile is rescaled to the interval $[-\pi, \pi]$. Typical testing samples are shown in Fig. 3a and Fig. 3b. In generating the simulated diffraction patterns, the probe pans across the illuminated object in known grid positions. However, in the reconstruction the measured diffraction patterns are accessed in a random sequence reduce the appearance of fictitious periodic artefacts in reconstruction [7].

In the present case, the probe is taken to have a flat top profile, generated from a coherent Gaussian profiled beam propagated

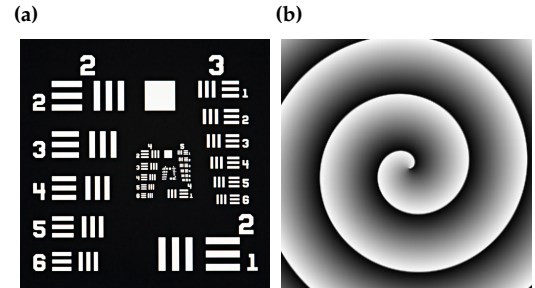


Fig. 3 (a) Sample amplitude chosen as USAF resolution test target, typically used to analyze and validate imaging systems
(b) Sample phase taken as a log spiral

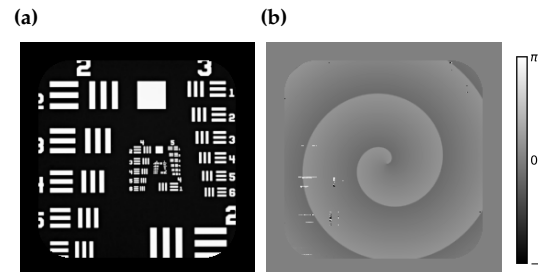


Fig. 4 Reconstructions of the object's amplitude (a) and phase (b) as shown in Fig. 3 after 30 iterations of an instance of the PIE algorithm.

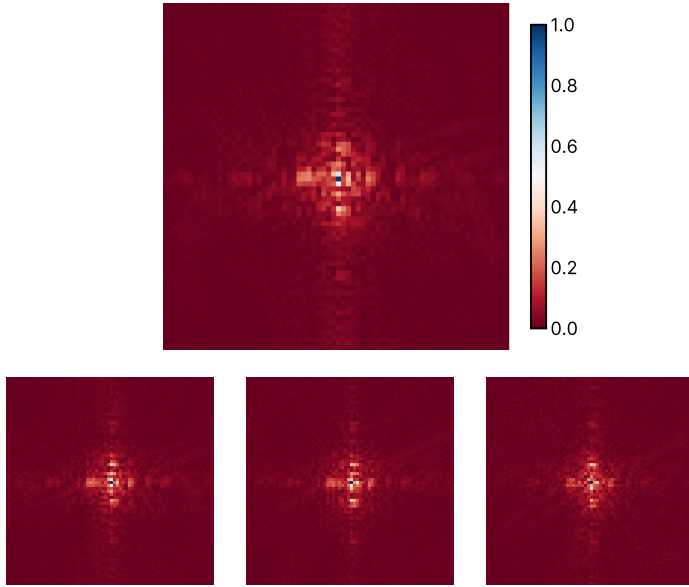


Fig. 5 A typical set of simulated diffraction patterns generated by the illuminating beam incident on the regions of interest on an object.

through suitable optics including a pinhole aperture a short distance from the object of interest. Further, the probe is assumed to have zero phase. In Fig. 4, I show the results of a typical run of the algorithm for 30 iterations. Here, the probe beam with a diameter of 70 pixels pans across 10×10 grid of known probe positions situated roughly in the center of the illuminated object. The spacing between the grid positions is 5 pixels, thus the probe positions go from (20, 20) to (165, 165); producing roughly a $\approx 93\%$ overlap between neighboring probe positions. Furthermore, the values of α, β in the object update function are both taken to zero; unless stated otherwise, all the given parameters here will remain unchanged.

The regions spanned by the illuminating beam are shown in Fig. 4 and also a typical set of simulated diffraction patterns is shown in Fig. 5. The diffraction patterns are masked to include only the regions illuminated by the probing beam. Thus in the present case, the patterns will be 70×70 pixels. This is simply a choice we make for computational convenience. In practice this is determined by the size of the active region of the detector, here also can consider a region of interest around the center of detector and discard pixels outside this region for reasons alike. As can be seen on Fig. 4, the algorithm under such idealized conditions faithfully recovers both the illuminated object's amplitude and phase in the regions of illumination. However, in the reconstructed phase one notices traces of pixels that seem to belong to the object's amplitude.⁶

⁶ This is an instance of *cross-talk* between the phase and amplitude parts of the object reconstruction as noted in Ref.[5]

2.2 Extended ptychography iterative engine (ePIE)

Introduced in Ref.[5], the extended ptychography iterative engine builds on the PIE algorithm and additionally reconstructs the illuminating beam in both amplitude and phase in conjunction with the illuminated object as described in section[1]. To probe the capabilities of the reconstruction, the illuminating beam is given a phase profile as shown in Fig. 6.

Out of the 30 iterations, the initial 5 are PIE iteration where only the estimate of the object is updated while probe estimate remains fixed (free space); only the remaining 25 iterations are both estimates update, everything else remains unchanged. The initial iterations are meant to start off the probe reconstruction with an estimate of the object that is not just free space (zero matrix), if not done the probe update function gives raise to divergences which make the reconstruction invalid. Fig. 7 shows the ePIE reconstructions.⁷

3 Quantitative rule of thumb for algorithmic convergence

SEEING THAT THE TWO ALGORITHMS, PIE and ePIE, produce reconstructions of the illuminated object and illuminating probe that have a resemblance to the originals, how do we decide whether the algorithms were successful or not in their reconstruction? Ref.[5] define a root-mean-square(RMS) error metric based on the true object amplitude and phase profile $O(\mathbf{r})$ as

$$E_O(n) = \frac{\sum_{\mathbf{r}} |O(\mathbf{r}) - \gamma O_n(\mathbf{r})|^2}{\sum_{\mathbf{r}} |O(\mathbf{r})|^2} \quad (15)$$

where γ is a phase offset defined by

$$\gamma = \frac{\sum_{\mathbf{r}} |O(\mathbf{r})O_n^*(\mathbf{r})|^2}{\sum_{\mathbf{r}} |O(\mathbf{r})|^2} \quad (16)$$

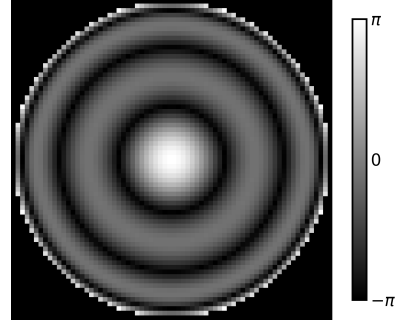


Fig. 6 Illuminating beam phase profile. This phase profile is based on profile of one of the Zernike polynomials $Z_n^m(\rho, \phi)$ with OSA and ANSI indices of $m, n = 6, 0$

⁷ Cross-talk between amplitude and phase reconstructions is much more pronounced here than in the PIE reconstructions as seen in Fig. 4

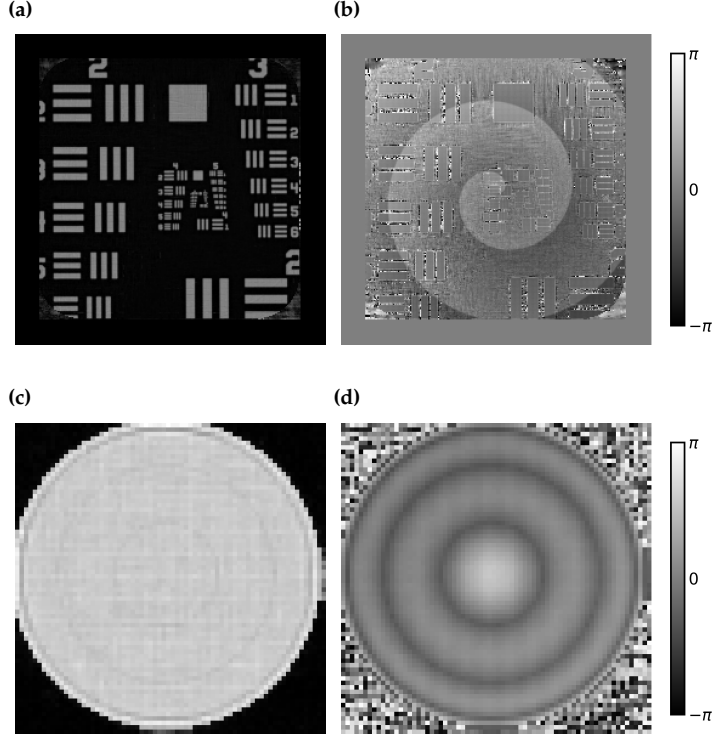


Fig. 7 (a) Object amplitude (b) Object phase (c) Probe amplitude and (d) Probe phase reconstructions after 5 PIE and 25 ePIE iterations.

and $O_n(\mathbf{r})$ is the object reconstruction after each diffraction patterns has been used in n times. Fig. 8 shows plots of $E_O(n)$ for 30 iterations of ePIE reconstructions of the objects described in the preceding subsection. The first 5 iterations during which the probe isn't updated, there aren't significant changes to the RMS errors. After this initial phase, the errors significantly decrease and subsequently converge to a fixed value, after roughly 15 iterations.

$$R(n) = \frac{\sum_{\mathbf{r},j} |\sqrt{I_{(n,j)}(\mathbf{r})} - \mathcal{F}(\psi_{(n,j)}(\mathbf{r}))|}{\sum_{\mathbf{r},j} \sqrt{I_{(n,j)}(\mathbf{r})}} \quad (17)$$

In describing the performance of the reconstruction in simulation, the error metric described above is a suitable metric of the convergence of the reconstructions. However, in practice one does not know the true object $O(\mathbf{r})$ so computing RMS error from Eq. 15 is not possible. Ref.[7] suggests the use of another error metric, called the "R-factor", which in the present case takes the following form

Fig. 9 shows plots of the R-factor for a set of four sample runs. The plots of the R-factor are in close agreement with those of Fig. 8; The errors significantly decrease after the first 5 iterations and stably

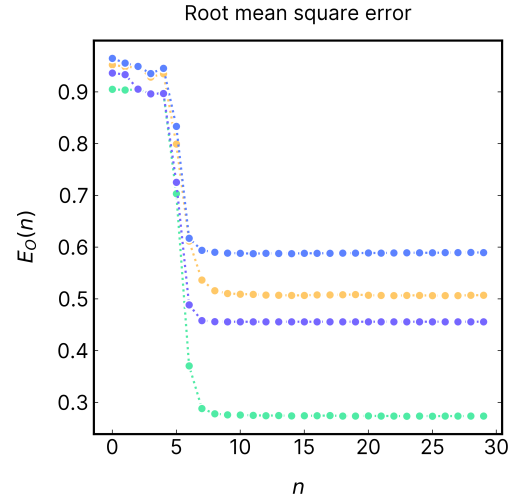


Fig. 8 RMS error metric as defined in eq.[15] for a set of ePIE reconstructions; a typical example seen in fig.[7]

settled onto a fixed value in a similar fashion.

4 Enhancements of the ptychography iterative engine

Ref.[8] studied how are the various parameters, particularly α, β , affect the reconstruction and subsequently proposed revisions to the original PIE and ePIE schemes to improve the reconstruction. One of first revisions proposed is that of the object and probe update functions; they suggest an update functions that take the form

$$O_{j+1}(\mathbf{r}) = O_j(\mathbf{r}) + \frac{P_j^*(\mathbf{r})(\psi'_j(\mathbf{r}) - \psi_j(\mathbf{r}))}{(1 - \alpha)|P_j(\mathbf{r})|^2 + \alpha|P_j(\mathbf{r})|_{\max}^2} \quad (18)$$

$$P_{j+1}(\mathbf{r}) = P_j(\mathbf{r}) + \frac{O_j^*(\mathbf{r})(\psi'_j(\mathbf{r}) - \psi_j(\mathbf{r}))}{(1 - \beta)|O_j(\mathbf{r})|^2 + \beta|O_j(\mathbf{r})|_{\max}^2} \quad (19)$$

The modified denominator in the new update functions is a convex combination of the modulus of the current probe estimate $|P_j(\mathbf{r})|$ and the maximum probe estimate value $|P_j(\mathbf{r})|_{\max}$. The modulus of the current probe estimate which considered alone simply divides out the current probe estimate from updated exit wave is believed to work quite well in illuminated regions with high intensity but otherwise ill-conditioned, for this reason the second term is added to counterbalance and reduce ill-conditioned of the first term in low intensity regions. The modifications to object and probe update functions as in Eq. 18 acquire the name regularized PIE (rPIE).

In the comparison of the different object update functions and their dependence on the parameters α, β in Ref.[8], they found that values $\alpha > 1$ the update functions of ePIE and PIE bias illuminated high-intensity regions, and thus low-intensity get comparably less frequent updates and small values of α worsen the convergence rate. On the other hand, rPIE is stable and performant even for much smaller values of α 0.05 and for values $0.05 < \alpha < 0.26$ give desirable condition where regions in between the two extremes (high- and low-intensity) are given heavier weights than in both ePIE and PIE. Lastly, they recommend setting $\beta = 1$, which is equivalent to ePIE probe update function, as they conclude it works well.

In addition to enhancements that don't involve the fine-tuning of α, β , they further describe two more modification to the probe update function. One is the correction the probe's intensity against a reference diffraction pattern $I_{\text{ref}}(\mathbf{r})$ to limit the effect of scaling and lateral shifts ambiguities of Eq. 3, 4. The intensity correction is done just before the probe and object updates in Eq. 18.

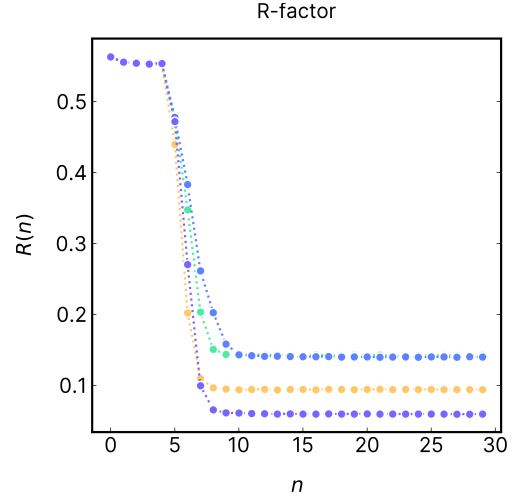


Fig. 9 R-factor as defined in Eq. 17 for a set of ePIE reconstructions

$$P_j(\mathbf{r}) = P_j(\mathbf{r}) \sqrt{\frac{\sum_{\mathbf{r}} |I_{\text{ref}}(\mathbf{r})|^2}{NM \sum_{\mathbf{r}} |P_j(\mathbf{r})|^2}} \quad (20)$$

where $N \times M$ is the number of pixels of the diffraction patterns. We choose $I_{\text{ref}}(\mathbf{r})$ to be brightest diffraction pattern in the set.

The second and last modification is that which reduces the global translation ambiguity by penalizing high probe intensities and incentivizes the probe to center in the reconstruction. This is done by modifying the rPIE probe update function in Eq. 18 as follows

$$P_{j+1}(\mathbf{r}) = P_j(\mathbf{r}) + \frac{O_j^*(\mathbf{r})(\psi'_j(\mathbf{r}) - \psi_j(\mathbf{r})) - b(\mathbf{r})P_j(\mathbf{r})}{(1 - \beta)|O_j(\mathbf{r})|^2 + \beta|O_j(\mathbf{r})|_{\max}^2 + b(\mathbf{r})} \quad (21)$$

where $b(\mathbf{r})$ is a mask with zeros in the intense region of the probe and gradually larger values are the edges and outside this region (i.e binary mask with zeros in the intense region and zeros outside it), in this high intensities regions are penalized towards the boundary of the intense region.

Fig. 10 shows plots of Eq. 15 after making incorporating all the enhancements described here and setting $\alpha = 0.15, \beta = 1.0$. In comparison to the plots in Fig. 8, we notice that the RMS error for a typical run is much reduced improved. However, this occurs the expense of the convergence not being as stable as in PIE and ePIE; The errors start to accumulate again after reaching a local minimum. The performance of rPIE algorithm is cited to be sensitive to the diffraction pattern order in the reconstruction [8]. One notices the artefacts in the amplitude profile of the reconstructed probe in Fig. 11, in some runs the artefacts do not show up at all and thus we suspect their due to the sensitive of the reconstruction to the order in which diffraction patterns are used in the reconstruction.

5 With different probing beams

The iterative engines (PIE, ePIE and rPIE) are cited to handle any form that the illuminating probe may assume, and not only restricted to flat-top probes; The only constraint is the probe should be localized [3]. In this section, we briefly explore ptychography reconstructions with different probing beams, particularly those composed of Gaussian-Laguerre and Gaussian-Hermite modes.

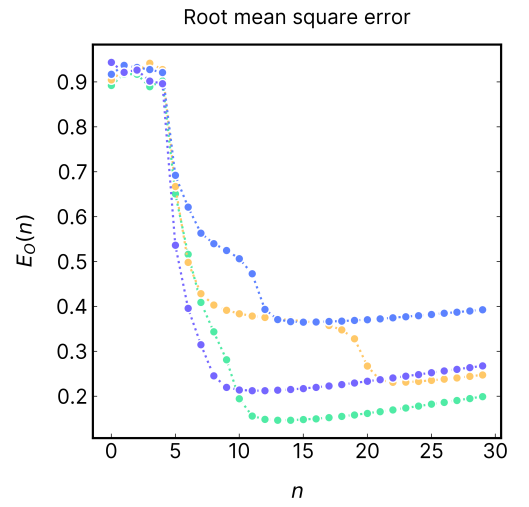


Fig. 10 RMS error metric for a set of reconstructions after making the modifications as described in this section

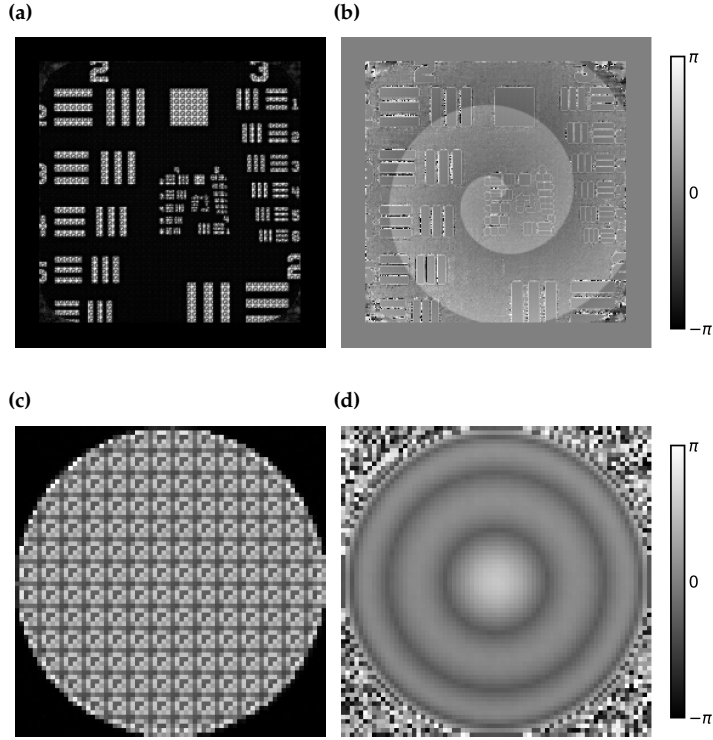


Fig. 11 (a) Object amplitude
(b) Object phase (c) Probe amplitude and (d) Probe phase reconstructions after 5 PIE and 25 rPIE iterations with modifications described in this section.

5.1 Laguerre-Gaussian modes

Laguerre-Gaussian(LG) modes are family of laser modes that have a rotational symmetry along their axis of propagation, and thus described in cylindrical coordinates (ρ, φ, z) . The intensity profile of such a beam is Gaussian profile, i.e. decreases for points away from the center in the direction perpendicular to the direction of propagation. In addition, the modes are labelled with two integers; the radial quantum number $p \geq 0$ and the azimuthal quantum number l . In Fig. 12 we show some of the LG beams for different values of the aforesaid quantum numbers. For an exposition on the theory of fundamental laser modes, see Ref.[9]. We employ Ref.[10] modifications to the Laguerre-Gaussian modes in the paraxial regime, as noted that the standard approximation is inaccurate when the ratio of the curvature of the beam $R(z)$ and its radial ρ is small, i.e $R(z)/\rho \ll 1$.

We again procedure in the same way and look at the reconstructions as in the previous section but here instead replace our probing beam with one of the LG modes. Furthermore, we crudely approximate the effect of a circular aperture on modes by masking the modes with binary mask. We first choose the transverse fundamental mode $l = 0, p = 0$ as for the probing beam. We show a typical output

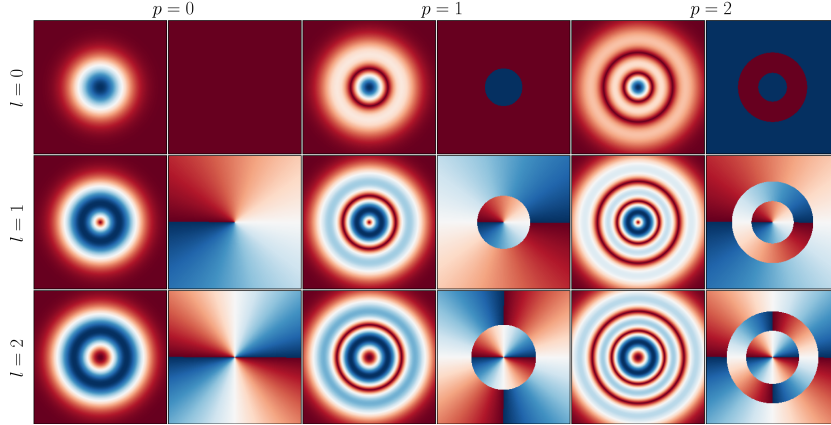


Fig. 12 The transverse spatial profiles of Laguerre-Gaussian modes in both intensity (left) and phase (right) for first three radial and azimuthal quantum numbers with $w_0 = 20 \mu\text{m}$, $\lambda = 624 \text{ nm}$ at $z \approx 0$. The diameter of the plot is $\approx 100 \mu\text{m}$

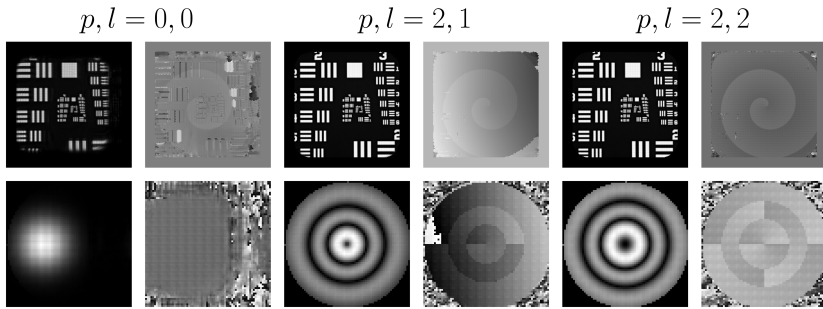


Fig. 13 Typical rPIE reconstructions of the object intensity (top left), phase (top right) and probing beam intensity (bottom left) and phase (bottom right) using the indicated LG modes as a probing beam.

of the reconstruction in Fig. 15. From these figure, we observe that the probing beams $p, l > 0$ the algorithmic is quite performant; giving a much improved resolution, in comparison to $p, l = 0, 0$, in both illuminated object and illuminating beam. We suspect that the increase in the orbital angular momenta of the beams results in larger diffraction angles, this in effect captures wider angular spectra / higher frequency components and subsequently improves the resolution of smaller structures on the sample [3].

6 With experimental errors

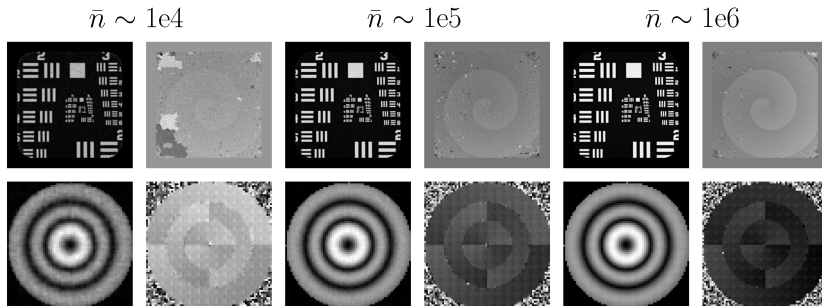
What has been investigated thus far is the behaviour and performance of the PIE, ePIE and rPIE algorithms under idealized operating conditions. However, in a real experiment various errors arise that deviate the operation of these algorithms away from its ideal operation. Under this section, we investigate some of these errors. This analysis closely follows that of reference [11].

6.1 Shot noise

In a real experiment the diffraction patterns are collected by a charge-coupled device (CCD) camera, which the basics of its operation are based on the photoelectric effect; Light incident on the camera induces the photosites (pixels) on the photoactive region of the camera accumulate electric charge (electron-holes) proportional to the light's intensity. Due to the corpuscular nature of this process and the independence of electric charges from one another, there arise statistical variations in the accumulation of these charges over a time interval (exposure time of the camera) and this variation is called shot noise, and such a statistical variation is described by the Poisson distribution. The pixel intensities vary according to this distribution.

$$P(n \text{ electrons in time interval } \Delta t) = \frac{(r\Delta t)^n e^{-r\Delta t}}{n!} \quad (22)$$

where r is the electron current in response to incident photon and Δt is the exposure time of the CCD camera. Suppose we consider values for $r\Delta t$ to range from $\sim 10^4$ to $\sim 10^6$.⁸



⁸ The quantity $\bar{n} = r\Delta t$ gives the average number of electrons detected during in the interval Δt

Fig. 14 rPIE reconstructions of the object intensity (top left), phase (top right) and probing beam intensity (bottom left) and phase (bottom right) in the presence of shot noise with indicated values for $\bar{n} = r\Delta t$

Low values of $r\Delta t$ lead to a decrease in accuracy of the reconstruction, while conversely high values improve the accuracy. Experimentally, if the value of r is fixed then value of the average electron count \bar{n} is influenced by the exposure time Δt . Thus short exposure time correspond to a decrease in accuracy in the output of the reconstruction, reference [11] cites this as due to the fact for short exposure time the fluctuations in the actual electron count is much increased than for long exposure times.

6.2 Random noise

In addition to shot noise, there could be other sources of noises in the experiment; pre-eminent, being from the surrounding environment influencing the physical process taking place in the experiment.

i.e. stray light entering the CCD camera or thermal fluctuations in the CCD camera could influence the pixel values of the diffraction patterns collected by the CCD camera. Reference [11] models kind of noise as random offset around a pixel value, *i.e.* for $0 < \nu < 1$, the pixel intensity I from a normalized diffraction pattern is offset by a value ν randomly assigned from the interval $[-\nu, \nu]$. We consider such a noise in addition to the shot noise with $\bar{n} \sim 1e6$.

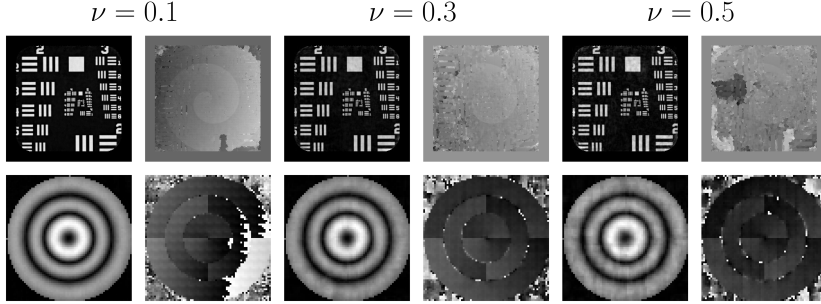


Fig. 15 rPIE reconstructions of the object intensity (top left), phase (top right) and probing beam intensity (bottom left) and phase (bottom right) in the presence of random pixel noise with indicated values for ν

We observe that the algorithm is robust against the two noise sources considered thus far, the reconstructed object and probe under the presence of shot noise for $\bar{n} \sim 1e6$ and random noise for $\nu = 0.30$ are quite discernible, with results only severely degrading at around $\nu = 0.5$. For an analysis of the other sources of possible errors we refer the reader to reference [11].

References

- [1] A. M. Maiden, J. M. Rodenburg, and M. J. Humphry. "Optical ptychography: a practical implementation with useful resolution". In: *Opt. Lett.* 35.15 (Aug. 2010), pp. 2585–2587. DOI: [10.1364/OL.35.002585](https://doi.org/10.1364/OL.35.002585). URL: <http://ol.osa.org/abstract.cfm?URI=ol-35-15-2585>.
- [2] R. J. M and H. M. L. Faulkner. "A Phase retrieval Algorithm for Shifting Illumination". English. In: *Applied Physics Letters* 85.20 (2004), pp. 4795–4797. ISSN: 0003-6951.
- [3] J. Rodenburg, A. Hurst, and A. Cullis. "Transmission microscopy without lenses for objects of unlimited size". In: *Ultramicroscopy* 107.2 (2007), pp. 227–231. ISSN: 0304-3991. DOI: <https://doi.org/10.1016/j.ultramic.2006.07.007>. URL: <https://www.sciencedirect.com/science/article/pii/S0304399106001549>.
- [4] P. Thibault, M. Dierolf, A. Menzel, O. Bunk, C. David, and F. Pfeiffer. "High-Resolution Scanning X-ray Diffraction Microscopy". In: *Science* 321.5887 (2008), pp. 379–382. ISSN: 0036-8075. DOI: [10.1126/science.1158573](https://doi.org/10.1126/science.1158573). eprint: <https://science.sciencemag.org/content/321/5887/379.full.pdf>. URL: <https://science.sciencemag.org/content/321/5887/379>.
- [5] A. M. Maiden and J. M. Rodenburg. "An improved ptychographical phase retrieval algorithm for diffractive imaging". In: *Ultramicroscopy* 109.10 (Sept. 2009), pp. 1256–1262. DOI: [10.1016/j.ultramic.2009.05.012](https://doi.org/10.1016/j.ultramic.2009.05.012). URL: <https://doi.org/10.1016%2Fj.ultramic.2009.05.012>.
- [6] J. Peatross and M. Ware. "Physics of Light and Optics: A Free Online Textbook". In: *Frontiers in Optics 2010/Laser Science XXVI*. Optical Society of America, 2010, JWA64. URL: <http://www.osapublishing.org/abstract.cfm?URI=LS-2010-JWA64>.
- [7] P. Thibault, M. Dierolf, O. Bunk, A. Menzel, and F. Pfeiffer. "Probe retrieval in ptychographic coherent diffractive imaging". In: *Ultramicroscopy* 109.4 (2009), pp. 338–343. ISSN: 0304-3991. DOI: <https://doi.org/10.1016/j.ultramic.2008.12.011>. URL: <https://www.sciencedirect.com/science/article/pii/S0304399108003458>.
- [8] A. Maiden, D. Johnson, and P. Li. "Further improvements to the ptychographical iterative engine". In: *Optica* 4.7 (July 2017), pp. 736–745. DOI: [10.1364/OPTICA.4.000736](https://doi.org/10.1364/OPTICA.4.000736). URL: <http://>

- //www.osapublishing.org/optica/abstract.cfm?URI=optica-4-7-736.
- [9] C. Koutschan, E. Suazo, and S. K. Suslov. "Fundamental laser modes in paraxial optics: from computer algebra and simulations to experimental observation". In: *Applied Physics B* 121.3 (Oct. 2015), pp. 315–336. ISSN: 1432-0649. DOI: 10.1007/s00340-015-6231-9. URL: <http://dx.doi.org/10.1007/s00340-015-6231-9>.
 - [10] J. Tuovinen. "Accuracy of a Gaussian beam". In: *IEEE Transactions on Antennas and Propagation* 40.4 (1992), pp. 391–398. DOI: 10.1109/8.138840.
 - [11] H. Faulkner and J. Rodenburg. "Error tolerance of an iterative phase retrieval algorithm for moveable illumination microscopy". In: *Ultramicroscopy* 103.2 (May 2005), pp. 153–164. DOI: 10.1016/j.ultramic.2004.11.006. URL: <https://doi.org/10.1016%2Fj.ultramic.2004.11.006>.